International Journal of Mass Spectrometry 297 (2010) 102–106

Contents lists available at ScienceDirect

International Journal of Mass Spectrometry

journal homepage: www.elsevier.com/locate/ijms

Infrared spectroscopic characterization of the oxidative dehydrogenation of propane by $V_4O_{10}^+$

Torsten Wende[a], Jens Döbler[b], Ling Jiang[a], Pieterjan Claes[c], Ewald Janssens[c], Peter Lievens[c], Gerard Meijer[a], Knut R. Asmis[a,*], Joachim Sauer[b,**]

[a] Fritz-Haber-Institut der Max-Planck-Gesellschaft, Faradayweg 4-6, D-14195 Berlin, Germany
[b] Institut für Chemie, Humboldt-Universität Berlin, Unter den Linden 6, D-10099 Berlin, Germany
[c] Laboratory of Solid State Physics and Magnetism & Institute for Nanoscale Physics and Chemistry (INPAC), K.U. Leuven, Celestijnenlaan 200d, B-3001 Leuven, Belgium

ARTICLE INFO

Article history:
Received 3 May 2010
Received in revised form 23 June 2010
Accepted 24 June 2010
Available online 3 July 2010

Keywords:
Vanadium oxide
Cluster structure
Cluster reactivity
Infrared photodissociation
Density function theory
Oxidative dehydrogenation

ABSTRACT

The gas phase reaction of $V_4O_{10}^+$ with propane is studied by infrared photodissociation spectroscopy combined with density functional calculations. Mass-selected $V_4O_{10}^+$ clusters react with propane under thermalized, multiple collision conditions in a buffer gas filled ion trap at 100 K. Two main reaction paths are identified: (i) oxidative dehydrogenation forming $V_4O_8(OH)_2^+$ + propene and (ii) direct dissociation leading to formation of $C_3H_7^+ + V_4O_9OH$. Formation of propene is effectively barrierless in the case that the initial H-atom is abstracted from a secondary C-atom. The present results highlight the additional structural information that can be gained from vibrational spectroscopy in comparison to a purely mass spectrometric characterization.

1. Introduction

Supported vanadium oxide particles are used as oxidation catalysts in various large scale industrial processes such as the conversion of SO_2 to SO_3, the formation of maleic anhydride from butane, and the oxidative dehydrogenation of propane. Despite their widespread use, the nature of the active sites, as well as the mechanistic details of the catalyzed oxidation reactions are far from understood, which hinders the development of tailored catalysts with increased yield and selectivity.

Characterization of structure–reactivity correlations, identification of reaction intermediates, and investigation of cluster size effects is important in providing fundamental knowledge, necessary to develop more efficient and more selective oxidation catalysts. In this respect gas-phase studies are important. They allow studying the intrinsic reactivity of the metal oxide in the absence of a support and of aggregation effects. While gas phase cluster experiments do not give conditions close to those in industrial catalytic processes, the high degree of control attainable allows careful investigation of the influence of particle composition, size, charge state, and temperature [1]. At the same time these systems are amenable to higher level quantum chemical approaches and the gas phase experimental results can provide benchmarks for the more approximate models applicable to condensed phase systems.

The chemical reactivity of gas phase size-selected vanadium oxide clusters with hydrocarbons was systematically investigated experimentally [2–14] and computationally [11,13,15–17] by several groups, demonstrating that their reactivity delicately depends on cluster size, charge state and stoichiometry. Vanadium oxide cations can react with alkanes and alkenes along several reaction pathways including: (i) molecular association, (ii) charge transfer, (iii) dehydrogenation, (iv) oxygen loss, (v) C–C bond cleavage and (vi) oxidative dehydrogenation (ODH). $V_4O_{10}^+$ was predicted to be particularly reactive [18] and indeed found to dehydrogenate methane under thermal conditions [10]. Upon reaction with propane ODH is the main channel and involves the transfer of two H atoms to the cluster, forming $[V_4O_{10}H_2]^+$ concomitant with the elimination of propene [12].

A more detailed insight into the molecular level mechanisms governing these gas phase reactions is clearly of interest, but difficult to extract from mass spectrometric measurements alone. Spectroscopic measurements, in combination with density functional calculations, have proven valuable to determine structures of anionic [19–24], neutral [25,26] and cationic [22,23,27–29] vana-

* Corresponding author. Tel.: +49 30 8413 5735; fax: +49 30 8413 5603.
** Corresponding author.
E-mail addresses: asmis@fhi-berlin.mpg.de (K.R. Asmis), js@chemie.hu-berlin.de (J. Sauer).

1387-3806/$ – see front matter © 2010 Elsevier B.V. All rights reserved.
doi:10.1016/j.ijms.2010.06.033

dium oxide clusters, but have rarely been extended to metal oxide cluster–hydrocarbon complexes. Fielicke et al. measured infrared photodissociation (IRPD) spectra of the association complex of $V_2O_{5,6}^+$ with ethylene formed in the expansion of the laser vaporization source [30]. These conditions were found to favor formation of the primary collision complex, rather than any reaction products.

Here we report on the reaction of mass-selected gas phase $V_4O_{10}^+$ clusters with propane under thermalized, multiple collision conditions in a buffer gas filled ion trap at 100 K. A tandem-mass spectrometer ensures that the mass of the charged reactants and products is well defined. In contrast to previous mass spectrometric work performed under single collision conditions [12], most clusters in our experiments are fully thermalized prior to a collision with a propane molecule through many collisions with He atoms, whose velocity distribution is determined by the ion trap temperature. The main reaction product, $[V_4O_{10}H_2]^+ \cdot C_3H_8$, is studied with IRPD spectroscopy, which, in combination with DFT calculations, provides a fingerprint of its structure. It is shown that such results represent a delicate probe for the validity of calculated reaction pathways and the predicted reaction mechanism.

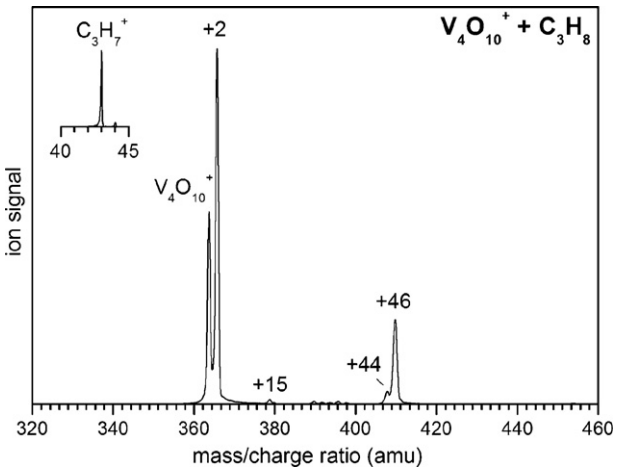

Fig. 1. Time-of-flight mass spectrum of all trapped ions after reaction of mass-selected $V_4O_{10}^+$ with 0.002% propane in He for a reaction time of 98 ms and at an ion trap temperature of 100 K. Only those parts of the mass spectrum are shown, where ion signal is observed. Numbers refer to mass differences with respect to $V_4O_{10}^+$ (364 amu).

2. Materials and methods

IRPD experiments [22,23,31,32] were carried out on a previously described ring electrode trap – tandem mass spectrometer [33,34], which was temporarily installed at the "Free Electron Laser for Infrared eXperiments" (FELIX) user facility [35] in the FOM Institute Rijnhuizen (The Netherlands).

The vanadium oxide clusters are produced with a repetition rate of 10 Hz by pulsed laser vaporization of a vanadium target in the presence of 0.1% O_2 in helium, yielding oxygen saturated cluster growth conditions [36]. The pulsed beam of positive ions is transferred into the high vacuum system, sampled by a 4 mm diameter skimmer, and focused into a radio frequency (RF) linear ion guide. $V_4O_{10}^+$ ions are mass-selected in a quadrupole mass filter with unit mass resolution, deflected 90° by an electrostatic quadrupole ion deflector and focused into the linear, ring electrode RF ion trap. The ions are accumulated and thermalized to the ambient temperature in the trap held at 100 K for 98 ms. The trap is filled with helium buffer gas containing 0.002–0.01% propane. The pressure inside the trap was not measured directly, but can be inferred from comparable experiments to be ~0.01–0.1 mbar [27]. At 0.02 mbar a $V_4O_{10}^+$ molecule experiences more than 10^4 hard-sphere collisions with He atoms and on average eight collisions with propane molecules while it is trapped. Such multiple collision conditions combined with the highly diluted gas mixture ensure thermalization of most of the reactants before the reaction occurs.

After storing the ions for 98 ms, all ions are extracted from the ion trap and focused both temporally and spatially into the center of the extraction region of an orthogonally mounted linear time-of-flight (TOF) mass spectrometer. Here, the ion packet can be irradiated with the pulsed radiation from FELIX and high voltage pulses are applied for the measurement of the TOF mass spectra. FELIX macropulses were produced at 5 Hz with a pulse length of 5 μs, a bandwidth of the laser wavelength over the range from 420 to 1200 cm^{-1} of ca. 0.2% RMS and typical pulse energies of up to 35 mJ. The FELIX beam was not focused in order to avoid saturation and ensuring low enough photon fluences, such that only weakly-bound clusters are photodissociated. IRMPD spectra are obtained in the difference-mode of operation. While FELIX runs at a repetition rate of 5 Hz, clusters are produced at 10 Hz. Hereby mass spectra are obtained, alternatively with and without interaction with the laser pulse, for a fixed wavelength. The two spectra are then subtracted. This cycle is performed 50–70 times for each wavelength step. IRMPD spectra are obtained from the difference mass spectra by plotting the intensity for a particular ion mass as a function of the photon energy.

3. Computational method

The DFT calculations are carried out using the TURBOMOLE program [37–39]. The B3LYP hybrid functional [40–42] is employed. The TZVP basis sets applied are the triple-zeta valence basis sets developed by Ahlrichs and coworkers [43] augmented by polarization functions, a d-set for oxygen and a p-set for vanadium [44], [5s, 3p, 1d] and [6s, 4p, 3d] for O and V, respectively. Structure optimizations use tight convergence criteria. Dispersion interaction was treated with the approach of Grimme [45,46], as implemented in TURBOMOLE 6.1. Structures are optimized until Cartesian gradients are smaller than 1×10^{-4} Hartree/Bohr and the energy change is smaller than 1×10^{-6} Hartree. The SCF convergence criterion is 1×10^{-7} Hartree for the energy and 1×10^{-7} a.u. for the root mean square of the density. Harmonic vibrational frequencies are obtained numerically from analytic gradients [47]. It is known that B3LYP vibrational frequencies are systematically too large (see e.g., Refs. [48,49]) and, therefore, agreement with observed frequencies can be improved by scaling. Scaling accounts for both anharmonicities and systematic errors of the calculated harmonic force constants (calculated harmonic wave numbers are compared to observed fundamentals including anharmonicities). We use scaling parameters [29] that we determined for small vanadium oxide cluster cations. Vanadyl modes are scaled by 0.9167 and all other modes by 0.9832.

4. Results and discussion

4.1. Mass spectrometry

A typical mass spectrum measured after the ion-molecule reactions of $V_4O_{10}^+$ with the 0.002% propane/helium gas mixture at 100 K is shown in Fig. 1. The parent ions correspond to the peak at 364 amu. Large intensities are found at +2 and +46 amu with respect to the parent ion peak, as well as at 43 amu. These peaks correspond to the formation of $[V_4O_{10}H_2]^+$, $[V_4O_{10}H_2C_3H_8]^+$, and $C_3H_7^+$, respectively. Minor peaks are observed at +15 ($[V_4O_{10}CH_3]^+$) and +44 amu ($[V_4O_{10}C_3H_8]^+$), as well as 44 amu ($C_3H_8^+$). At slightly higher ion trap temperatures (110 K) and higher propane concen-

trations (0.01% propane in He) the intensity of the parent ion peak is reduced considerably, while the peak at +46 amu increases in intensity. In addition, a new peak appears at +90 amu, corresponding to the formation of $[V_4O_{10}H_2(C_3H_8)_2]^+$. Summarizing, the following set of reactions explains the observed mass spectrum

$$V_4O_{10}^+ + C_3H_8 \rightleftarrows (V_4O_{10}\cdot C_3H_8)^+ \quad (1)$$

$$(V_4O_{10}\cdot C_3H_8)^+ \rightarrow V_4O_9OH + C_3H_7^+ \quad (2A)$$

$$(V_4O_{10}\cdot C_3H_8)^+ \rightarrow [V_4O_{10}H_2]^+ + C_3H_6 \quad (2B)$$

$$(V_4O_{10}\cdot C_3H_8)^+ \rightarrow [V_4O_{10}CH_3]^+ + C_2H_5 \quad (2C)$$

$$[V_4O_{10}H_2]^+ + C_3H_8 \rightleftarrows [V_4O_{10}H_2]^+\cdot C_3H_8 \quad (3B)$$

$$[V_4O_{10}H_2]^+\cdot C_3H_8 + C_3H_8 \rightleftarrows [V_4O_{10}H_2]^+\cdot (C_3H_8)_2 \quad (4B)$$

The present results are in good agreement with the previously reported mass spectrometric data by Feyel et al. [12], which were measured under single collision conditions and at room temperature, if the different experimental conditions are taken into consideration. (a) In both experiments the main product ions detected are $[V_4O_{10}H_2]^+$ and $C_3H_7^+$. (b) Thermalization at low temperatures via many collisions with the He atoms allows stabilizing weakly-bound complexes, which are not observed in the room temperature measurements, like the encounter complex $(V_4O_{10}\cdot C_3H_8)^+$ and the product ion–propane complexes $[V_4O_{10}H_2]^+\cdot(C_3H_8)_{1,2}$. The latter result from multiple collisions with propane molecules. (c) Formation of $V_4O_9^+$ is not observed in the present experiments, suggesting that the side reaction leading to the formation of $V_4O_9^+$ + propanol is suppressed. However, the $(V_4O_9\cdot C_3H_7OH)^+$ complex, which has the same mass as $(V_4O_{10}\cdot C_3H_8)^+$, may be present (see Section 4.3).

4.2. IRPD spectroscopy

Additional information can be gained from IRPD spectroscopy of the $[V_4O_{10}H_2]^+\cdot C_3H_8$ complex. Upon irradiation of the ion packet extracted from the ion trap under low photon fluence conditions, i.e., using an unfocused FELIX beam, a single photodissociation channel is observed, namely depletion of the signal at mass 410 amu ($[V_4O_{10}H_2]^+\cdot C_3H_8$) and concomitant formation of ions with mass 366 amu ($[V_4O_{10}H_2]^+$), which corresponds to the loss of a propane molecule. The weak signal at 408 amu ($[V_4O_{10}C_3H_8]^+$) is also depleted and leads to formation of mass 364 amu ($V_4O_{10}^+$), but its signal is too weak to yield a well resolved IR spectrum, also because of the significant change in signal at +2 amu, mentioned above. The ion signals observed at 43, 364, and 366 amu do not decrease in intensity, suggesting that these ions are bound too strongly to dissociate under the present conditions.

The IRPD spectrum of $[V_4O_{10}H_2]^+\cdot C_3H_8$, measured by monitoring the daughter ion signal (366 amu), is shown in the bottom part of Fig. 2. It is characterized by at least eight discrete absorption peaks, two characteristic vanadyl bands at 1049 and 1037 cm^{-1}, and six bands in-between 600 and 950 cm^{-1}, i.e., in the V–O–V stretching and C–C–H bending region. Simulated linear absorption spectra of three possible structural candidates, labeled A1, A2 and B, are plotted in the upper part of Fig. 2. Structures A and B differ in the number of vanadyl groups present in the $[V_4O_{10}H_2]^+$ moiety. While structure A contains two vanadyl and two V–OH groups, structure B contains three vanadyl and one V–OH_2 group. Structures A1 and A2, on the other hand, differ in how the propane molecule is bound to the $[V_4O_{10}H_2]^+$ complex, which influences the orientation of the V–OH groups relative to each other. Comparison of the experimental to the simulated spectra clearly favors an assignment to structures A1 and A2 rather than B. The simulated spectrum of B can neither account for the strongest absorption band at 889 cm^{-1}, nor for the two absorption bands in-between 730 and 780 cm^{-1}. In contrast, the A spectra do account for the absorption in these spectral regions and they also reproduce the relative intensities of the vanadyl bands satisfactorily. The larger width (~25 cm^{-1}) of the 889 cm^{-1} band compared to the other peaks (<15 cm^{-1}) in the experimental spectrum as well as the observation of two peaks of similar intensity in-between 730 and 780 cm^{-1} suggests that both isomers, A1 and A2, are formed and probed in the experiment. This is in agreement with calculated stabilities of A1 and A2, which differ by less than 1 kJ/mol, while B is 33 kJ/mol less stable. Several weaker absorption bands are predicted for all three structures below 700 cm^{-1}. The lowest energy feature observed in the experimental spectrum is at 651 cm^{-1}, suggesting that the photodissociation efficiency is significantly reduced below this energy.

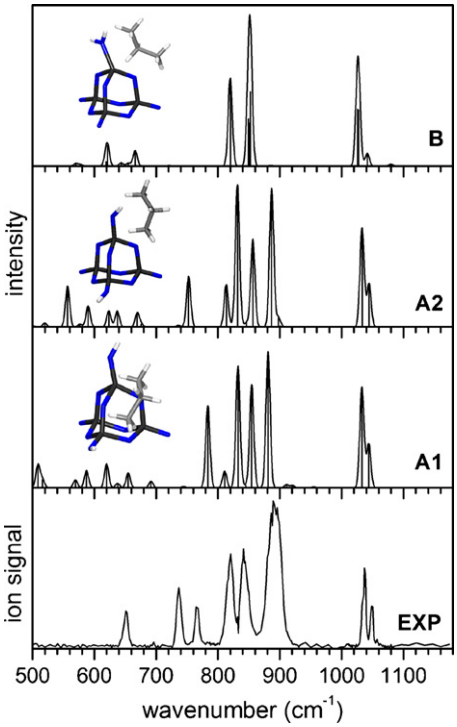

Fig. 2. Experimental IRPD spectrum (bottom) of the 410 amu → 366 amu channel, corresponding to C_3H_8 loss from $[V_4O_{10}H_2\cdot C_3H_8]^+$, after trapping mass-selected $V_4O_{10}^+$ ions (364 amu) at 100 K for 48 ms in the ion trap filled with a 0.002% propane in helium gas mixture. Simulated linear IR absorption spectra, derived from B3LYP/TZVP harmonic frequencies and intensities (see text), of three possible structural candidates, labeled B, A1 and A2, are also shown.

4.3. Reaction mechanism

Previously it was found that $V_4O_{10}^+$ abstracts hydrogen from methane without a barrier [10]. We expect that propane will react similarly, because its C–H bond dissociation energy is smaller, 411 and 395 kJ/mol for the primary and secondary C–H bonds, respectively compared to 435 kJ/mol for methane [50]. Another difference to methane is the lower ionization energy due to the inductive effect of the methyl groups. Whereas the *vertical* electron affinity (EA) of $V_4O_{10}^+$ (10.1 eV at the B3LYP/TZVP level) is still smaller than the *vertical* ionization energy (IE) for propane (11.5 eV) the adiabatic EA of $V_4O_{10}^+$ is significantly larger (11.1 eV) than the adiabatic IE of propane (10.6 eV) due to stronger relaxation. This explains that a calculation of $V_4O_{10}^+$ and propane at their equilibrium structures at a moderate fixed distance (structure **1** in Fig. 3, distance between vanadyl oxygen and hydrogen equals to 359 pm) yields a negative energy with respect to the reactants (−26 kJ/mol). In the adiabatic case electron transfer is preferred (IE − EA = −0.5 eV).

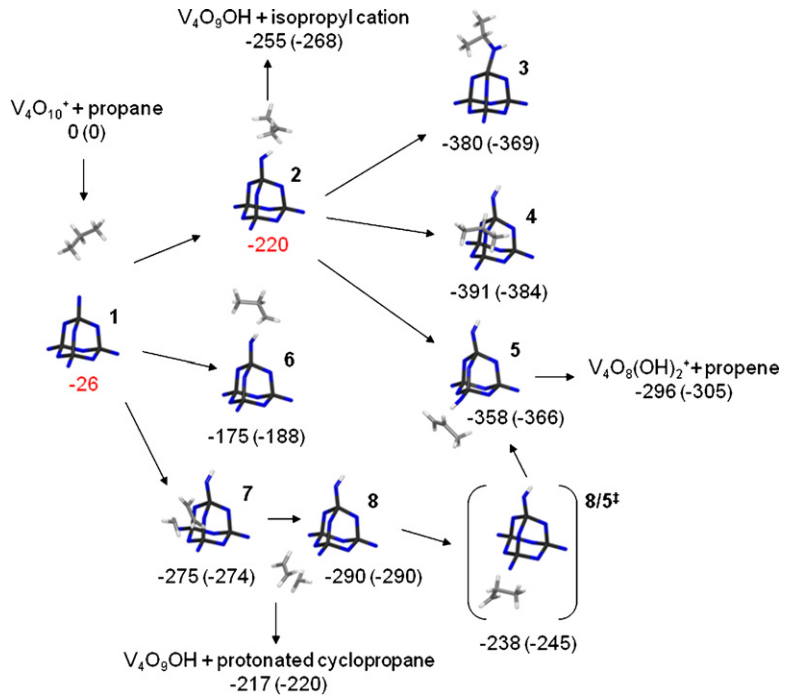

Fig. 3. Calculated B3LYP/TZVP energies (in kJ/mol) and structures and proposed reaction path for the formation of $V_4O_8(OH)_2(C_3H_8)^+$. The absorption of a first propane molecule is highly exothermic and goes over an intermediate complex to molecular hydrogen abstraction together with the release of propene. Upon collision with a second propane molecule the weakly bonded $V_4O_8(OH)_2(C_3H_8)^+$ complex is formed. Red numbers denote transient, non-equilibrium structures. Values including zero point vibration energy are given in parentheses.

Whereas for hydrogen abstraction from a primary C–H bond intermediate **6** could be identified that corresponds to a formal hydride transfer, for hydrogen abstraction from the secondary position no minimum structure for an intermediate was found. Structure **2** in Fig. 3 (220 kJ/mol below the reactants) is not a stationary point on the potential energy surface, but a point taken from an optimization run at which the gradient norm represents a local minimum, i.e., a point at which the slope towards the possible products is least steep. One possible reaction route is desorption, leading to V_4O_9OH and $C_3H_7^+$ with a reaction energy of $\Delta H_0 = -268$ kJ/mol. The formation of the carbocation is preferred, because the IE of C_3H_7 (7.6 eV) is lower than the EA of $V_4O_9OH^+$ (8.6 eV): Structure optimizations starting from the same structure **2** (but using different step sizes) yielded two different product structures. In one route isopropanol is formed by a rebound step in which the secondary carbon forms a bond with the hydroxyl oxygen atom (structure **3**, $\Delta H_0 = -369$ kJ/mol). In the second route, the hydrocarbon moves along a V–O–V bridge and the secondary carbon binds to the bridging oxygen, forming a bridging isopropoxy group (**4**, $\Delta H_0 = -384$ kJ/mol). A third possible route is hydrogen abstraction from the primary C–H bond by a vanadyl oxygen. This completes the ODH forming propene and $V_4O_8(OH)_2^+$ (structure **5**, $\Delta H_0 = -366$ kJ/mol). In all three optimizations a steady decrease of the energy was found, making it very likely that all three routes correspond to barrierless reaction paths.

Intermediate **6** formed by hydrogen abstraction from a primary carbon atom (Fig. 3) corresponds to an energy minimum structure ($\Delta H_0 = -188$ kJ/mol). It should be noted that the primary propyl cation does not exist as an isolated species in the gas phase (at least not at the B3LYP/TZVP level employed): optimization yields a secondary propyl cation due to a barrierless hydrogen transfer. The fact that a primary propyl species is present in **6** indicates that the ion is stabilized by intermolecular interaction with the OH bond formed. There is a second intermediate **7** (found by MD simulation starting from **1** followed by optimization) in which the propyl ion forms a cyclic structure that can be characterized as ethene, interacting with CH_3^+, positioned above the plane. ($\Delta H_0 = -274$ kJ/mol) The cyclic $C_3H_7^+$ ion also corresponds to a minimum structure of the isolated species in the gas phase, which is 48 kJ/mol less stable than the secondary propyl cation. Although the formation of **7** is not barrierless (otherwise **6** would not exist) the occurrence of this reaction in an MD run indicates that the barrier is small and the reaction route will be accessible under the current experimental conditions.

There is a somewhat more stable isomer of **7**, in which the protonated cyclopropane moiety does not interact with the V–O–V bridge, but with a vanadyl oxygen (**8**, $\Delta H_0 = -290$ kJ/mol). Differently from the isopropyl cation, this moiety does not rebind to oxygen sites of V_4O_9OH. Besides dissociation of **7** or **8** into V_4O_9OH + protonated cyclopropane ($\Delta H_0 = -220$ kJ/mol), from **8** the system may go through a transition structure (TS), **8/5‡** in Fig. 3, in which one hydrogen atom of the ethene moiety is bent out of the plane and the CH_3^+ moves towards one of the carbon atoms. The intrinsic barrier is 45 kJ/mol, but the energy of the TS is still 25 kJ/mol below the energy for dissociation of the protonated cyclopropane from the cluster. After going through the TS the system relaxes to $V_4O_8(OH)_2^+$ and propene.

5. Conclusion

The results of our calculations allow for a more detailed explanation of the products observed in the mass spectrum. As $V_4O_{10}^+$ and C_3H_8 approach each other, hydrogen abstraction accompanied by electron transfer, i.e., hydride transfer, will occur without a barrier. The reaction system can follow several paths. (a) Direct dissociation leads to formation of $C_3H_7^+$ (+V_4O_9OH) which is found experimentally as one of the major products. Since the vanadium oxide cluster is neutralized in this process, it is no longer confined by the trapping potentials, is lost from the trapping volume and is

not available for any further reactions. (b) Abstraction of a second H-atom forms $[V_4O_{10}H_2]^+$ ($+C_3H_6$) which is the dominant reaction observed in the experiment and selectively involves two vanadyl groups rather than a single one, as evidenced by the IRPD spectrum (structures A1 and A2 in Fig. 2). In the latter case a species containing an $–OH_2$ moiety would be formed (structure B in Fig. 2), which is neither observed in the experiment nor favored by the calculations.

Formation of propene is particularly probable for the case that the initial H-atom was abstracted from a secondary C-atom, in which case the process is effectively barrierless. Even though the binding energy of propene to $V_4O_8(OH)_2^+$ is 62 kJ/mol, the reaction proceeds sufficiently fast compared to the cooling rate ($10^4\,s^{-1}$) that the excess energy cannot be dissipated and the complex dissociates. Under the experimental conditions a vanadium oxide ion will, on average, experience several collisions with propane molecules and these lead to the formation of the observed, weakly-bound (∼29 kJ/mol per propane molecule) $V_4O_8(OH)_2^+\cdot(C_3H_8)_{1,2}$ complexes, which can be stabilized by three-body collisions.

Finally, it seems probable that the small mass peak at 408 amu ($[V_4O_{10}C_3H_8]^+$) corresponds to the isopropanol (**3**) and isopropoxy (**4**) products, rather than to the $(V_4O_{10}\cdot C_3H_8)^+$ (**1**) or $(V_4O_8(OH)_2\cdot C_3H_6)^+$ (**5**) complexes. The energy of dissociation into isopropanol and $V_4O_9^+$ is 241 kJ/mol and that of the bridging isopropoxy species into $V_4O_9OH + C_3H_7^+$ is 131 kJ/mol. The dissociation energies, in particular for isopropanol, are thus considerably larger than for the other two complexes, making their stabilization more probable. Although formation of the isopropanol and propoxy products is exothermic, it can be assumed that part of this energy is redistributed to other degrees of freedom and eventually lost in collisions with the buffer gas. The presence of isopropanol and isopropoxy products is also in agreement with the previous mass spectrometric studies under single collision conditions [12], where, in contrast to the present study, $V_4O_9^+$ is observed in small amounts.

Acknowledgements

The authors gratefully acknowledge the support of the Stichting voor Fundamenteel Onderzoek der Materie (FOM) in providing the required beam time on FELIX and highly appreciate the skillful assistance of the FELIX staff. The research leading to these results has received funding from the European Community's Seventh Framework Programme (*FP7*/2007–2013) under grant Agreement No. 226716 and from the German Research Foundation within the dedicated research center SFB-546. L.J. thanks the Alexander von Humboldt Foundation for a post doctoral scholarship. P.C. thanks the *Agency for Innovation by Science and Technology in Flanders* (*IWT*) for financial support. We acknowledge the preliminary work of Gabriele Santambrogio and thank him for helpful discussions.

Appendix A. Supplementary data

Supplementary data associated with this article can be found, in the online version, at doi:10.1016/j.ijms.2010.06.033.

References

[1] D.K. Böhme, H. Schwarz, Angew. Chem. Int. Ed. 44 (2005) 2336.
[2] R.C. Bell, K.A. Zemski, K.P. Kerns, H.T. Deng, A.W. Castlemann Jr., J. Phys. Chem. A 102 (1998) 1733.
[3] R.C. Bell, K.A. Zemski, A.W. Castleman Jr., J. Cluster Sci. 10 (1999) 509.
[4] R.C. Bell, A.W. Castleman, J. Phys. Chem. A 106 (2002) 9893.
[5] K.A. Zemski, D.R. Justes, A.W. Castleman, J. Chem. Phys. B 106 (2002) 6136.
[6] A. Fielicke, K. Rademann, Phys. Chem. Chem. Phys. 4 (2002) 2621.
[7] D.R. Justes, R. Mitrić, N.A. Moore, V. Bonačić-Koutecký, A.W. Castleman Jr., J. Am. Chem. Soc. 125 (2003) 6289.
[8] N.A. Moore, R. Mitrić, D.R. Justes, V. Bonačić-Koutecký, A.W. Castleman, J. Chem. Phys. B 110 (2006) 3015.
[9] M. Engeser, M. Schlangen, D. Schröder, H. Schwarz, Organometallics 22 (2003) 3933.
[10] S. Feyel, J. Döbler, D. Schröder, J. Sauer, H. Schwarz, Angew. Chem. Int. Ed. 45 (2006) 4681.
[11] S. Feyel, D. Schröder, X. Rozanska, J. Sauer, H. Schwarz, Angew. Chem. Int. Ed. 45 (2006) 4677.
[12] S. Feyel, D. Schröder, H. Schwarz, J. Phys. Chem. A 110 (2006) 2647.
[13] F. Dong, S. Heinbuch, Y. Xie, J.J. Rocca, E.R. Bernstein, Z.C. Wang, K. Deng, S.G. He, J. Am. Chem. Soc. 130 (2008) 1932.
[14] S.H. Li, A. Mirabal, J. Demuth, L. Wöste, T. Siebert, J. Am. Chem. Soc. 130 (2008) 16832.
[15] D.R. Justes, A.W. Castleman, R. Mitrić, V. Bonačić-Koutecký, Eur. Phys. J. D 24 (2003) 331.
[16] X. Rozanska, J. Sauer, J. Phys. Chem. A 113 (2009) 11586.
[17] X. Rozanska, J. Sauer, Int. J. Quantum Chem. 108 (2008) 2223.
[18] J. Sauer, J. Döbler, Dalton Trans. 19 (2004) 3116.
[19] H. Wu, L.-S. Wang, J. Chem. Phys. 108 (1998) 5310.
[20] H.J. Zhai, L.-S. Wang, J. Chem. Phys. 117 (2002) 7882.
[21] K.R. Asmis, G. Santambrogio, M. Brümmer, J. Sauer, Angew. Chem. Int. Ed. 44 (2005) 3122.
[22] K.R. Asmis, J. Sauer, Mass Spectrom. Rev. 26 (2007) 542.
[23] K.R. Asmis, J. Sauer, Mass Spectrom. Rev. 27 (2008) 205.
[24] G. Santambrogio, M. Brümmer, L. Wöste, J. Döbler, M. Sierka, J. Sauer, G. Meijer, K.R. Asmis, Phys. Chem. Chem. Phys. 10 (2008) 3992.
[25] I.R. Beattie, J.S. Ogden, D.D. Price, Inorg. Chem. 17 (1978) 3296.
[26] C. Herwig, C. Limberg, Inorg. Chem. 47 (2008) 2937.
[27] K.R. Asmis, M. Brümmer, C. Kaposta, G. Santambrogio, G. von Helden, G. Meijer, K. Rademann, L. Wöste, Phys. Chem. Chem. Phys. 4 (2002) 1101.
[28] M. Brümmer, C. Kaposta, G. Santambrogio, K.R. Asmis, J. Chem. Phys. 119 (2003) 12700.
[29] K.R. Asmis, G. Meijer, M. Brümmer, C. Kaposta, G. Santambrogio, L. Wöste, J. Sauer, J. Chem. Phys. 120 (2004) 6461.
[30] A. Fielicke, R. Mitrić, G. Meijer, V. Bonačić-Koutecký, G. von Helden, J. Am. Chem. Soc. 125 (2003) 15716.
[31] J. Oomens, B.G. Sartakov, G. Meijer, G. von Helden, Int. J. Mass Spectrom. 254 (2006) 1.
[32] J. Oomens, A.G.G.M. Tielens, B. Sartakov, G. von Helden, G. Meijer, Astrophys. J. 591 (2003) 968.
[33] D.J. Goebbert, G. Meijer, K.R. Asmis, AIP Conf. Proc. 1104 (2009) 22.
[34] D.J. Goebbert, T. Wende, R. Bergmann, G. Meijer, K.R. Asmis, J. Phys. Chem. A 113 (2009) 5874.
[35] D. Oepts, A.F.G. van der Meer, P.W. van Amersfoort, Infrared Phys. Technol. 36 (1995) 297.
[36] W. Bouwen, P. Thoen, F. Vanhoutte, S. Bouckaert, F. Despa, H. Weidele, R.E. Silverans, P. Lievens, Rev. Sci. Instrum. 71 (2000) 54.
[37] R. Ahlrichs, M. Bär, M. Häser, H. Horn, C. Kölmel, Chem. Phys. Lett. 162 (1989) 165.
[38] K. Eichkorn, O. Treutler, H. Öhm, M. Häser, R. Ahlrichs, Chem. Phys. Lett. 242 (1995) 652.
[39] O. Treutler, R. Ahlrichs, J. Chem. Phys. 102 (1995) 346.
[40] A.D. Becke, Phys. Rev. A 38 (1988) 3098.
[41] A.D. Becke, J. Chem. Phys. 98 (1993) 5648.
[42] C. Lee, W. Yang, R.G. Parr, Phys. Rev. B 37 (1988) 785.
[43] A. Schäfer, C. Huber, R. Ahlrichs, J. Chem. Phys. 100 (1994) 5829.
[44] A.J. Wachters, J. Chem. Phys. 52 (1970) 1033.
[45] S. Grimme, J. Comput. Chem. 25 (2004) 1463.
[46] S. Grimme, J. Comput. Chem. 27 (2006) 1787.
[47] P. Deglmann, F. Furche, R. Ahlrichs, Chem. Phys. Lett. 362 (2002) 511.
[48] A.P. Scott, L. Radom, J. Chem. Phys. 100 (1996) 16502.
[49] M.D. Halls, J. Velkovski, H.B. Schlegel, Theor. Chem. Acc. 105 (2001) 413.
[50] J.A. Kerr, Chem. Rev. 66 (1966) 465.